Journal of
Materials Chemistry C

Accepted Manuscript

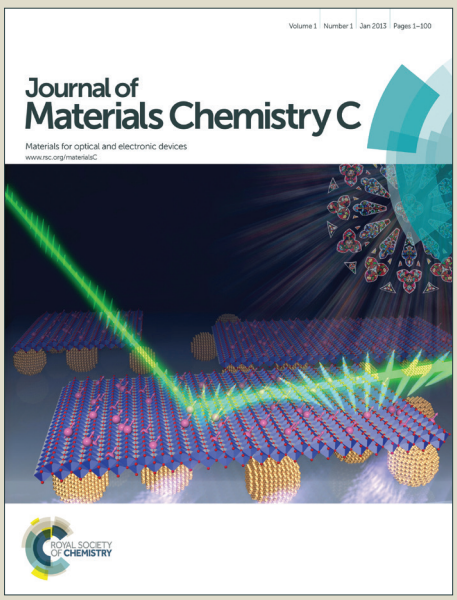

ROYAL SOCIETY OF CHEMISTRY

www.rsc.org/materialsC

Journal Name

ARTICLE

Evaluation of 1:2 Ordered Structure of $Ba(B'_{1/3}B''_{2/3})O_3$ Perovskites by TEM Observation along Various Zone Axes

Received 00th January 20xx,
Accepted 00th January 20xx

DOI: 10.1039/x0xx00000x

www.rsc.org/

Pian Pian Ma,[a] Hui Gu[b] and Xiang Ming Chen*[a]

The 1:2 ordered structure of $Ba(B'_{1/3}B''_{2/3})O_3$ perovskites has been intensively studied by transmission electron microscopy (TEM) observation from different projections ($<110>_c$, $<111>_c$ and $<112>_c$) in $Ba((Co, Zn, Mg)_{1/3}Nb_{2/3})O_3$ ceramics. For $<110>_c$ and $<112>_c$ zone axes, the occurrence of 1/3{111}-type superlattice reflections in their corresponding selected area electron diffraction (SAED) images directly reveals the 1:2 ordered structure. The most informative $<110>_c$ zone gives two sets of $<111>_c$ ordering variants, providing convenience to detect the twin boundaries. While $<112>_c$ zone axis with only one set of $<111>_c$ variant, has its own advantage to detect single anti-phase boundaries (APBs). In addition, $<111>_c$ zone axis, which is parallel to the ordering direction, clearly shows the hexagonal symmetry of 1:2 ordered structure in the corresponding HRTEM image. For a completely ordered sample, there are always a certain proportion of areas without superperied lattice. These areas should also be the ordered domains, whose variants are not perpendicular to the given zone axis.

Introduction

Complex perovskites with chemical formula $Ba(B'_{1/3}B''_{2/3})O_3$ (B' = Zn^{2+}, Mg^{2+}, Co^{2+} and Ni^{2+}, B'' = Ta^{5+}, Nb^{5+}) and their solid solutions have attracted considerable interest acting as filters, resonators and tuners in cellular communication industry due to their excellent dielectric properties in the microwave frequency range.[1-3]

For $Ba(B'_{1/3}B''_{2/3})O_3$ perovskites, when two B-site species distribute randomly, it shows cubic structure with $Pm\bar{3}m$ symmetry (lattice parameter a_c). However, an ordered B-site arrangement with a ({…B'- B''- B''…}) repeat sequence is usually stabilized when the two species differ sufficiently in their valence, size or coordination preference.[4-5] It gives rise to a hexagonal ($P\bar{3}m1$) superstructure with lattice parameters $a_h=\sqrt{2}a_c$ and $c_h=\sqrt{3}a_c$.[6]

The 1:2 ordering forms along an arbitrary [111] direction of the parent cubic cell, which is coincident with the c direction of the supercell.[7-9] It is worth noting that there are four possible equivalent $<111>_c$ (subscript c indicates cubic) variants for B-site ordering.[8,10] During the ordering process, two different types of ordered domain boundaries are possible. 1) 71/109° twin boundaries between regions that have nucleated in phase but on different sets of $\{111\}_c$ planes; 2) Anti-phase boundaries (APBs) between regions that have nucleated on the same set of $\{111\}_c$ planes but out of phase.[7,11] These two kinds of domain boundaries are very common in $Ba(B'_{1/3}B''_{2/3})O_3$ perovskites.

According to Schlömann's theory, dielectric loss of materials increases when cations distribute disorderly because the periodic arrangement of charges in the crystal is broken.[12-13] It is well-supported in $Ba(B'_{1/3}B''_{2/3})O_3$ perovskites that 1:2 ordered sample exhibits a much higher Qf value than the disordered one.[14-15] The higher B-site ordering degree, the lower dielectric loss. Besides the B-site ordering degree, the ordering-induced domain structure has also been proved to have significant effects on the microwave dielectric properties, especially the Qf value.[16-18] The effect on Qf value caused by twin boundaries has been reported in our previous work. Four

[a] Laboratory of Dielectric Materials, School of Materials Science and Engineering, Zhejiang University, Hangzhou 310027, CHINA. E-mail: xmchen59@zju.edu.cn
[b] School of Materials Science and Engineering, Materials Genome Institute, Shanghai University, Shanghai 200072, CHINA

types of twin boundaries with different orientations have been detected, and the energy determined by the cation disruption at the interface has a direct relationship with quality factor.[9] While the effect caused by APBs is still controversial. However, it is certain that the stabilization of the domain boundaries (twin boundaries and APBs) can reduce the driving force of ordering domain growth and minimize the dielectric loss.[11,17] Thus, a better understanding of the ordered structure contributes significantly to the property optimization and structure design for $Ba(B'_{1/3}B''_{2/3})O_3$ perovskites.

To determine the 1:2 ordered structure, X-ray diffraction (XRD) is the most convenient tool and used quite commonly. However, the detection of ordering by XRD is often limited by the volume fraction and the scattering factor difference between two *B*-site species. In addition, the ordering signatures from XRD is an average state of the whole sample, more details about the local ordering characteristics are overlooked. However, the availability of transmission electron microscopy with atom level resolution overcomes the problems associated with XRD and has provided a direct means to detect the noteworthy microstructures of these structurally $Ba(B'_{1/3}B''_{2/3})O_3$ complex perovskites.[17-21]

$Ba((Co, Zn, Mg)_{1/3}Nb_{2/3})O_3$ belongs to the family of $Ba(B'_{1/3}B''_{2/3})O_3$ perovskites. Their ordering features and excellent microwave dielectric properties have been discussed in our previous work.[9,22] Since Nb and Ta belong to the same period and have the same ionic radius (r = 0.640 Å)[23], $Ba(B'_{1/3}Nb_{2/3})O_3$ and $Ba(B'_{1/3}Ta_{2/3})O_3$ show great similarity in structural transformation and resulting properties. Moreover, the TEM observation for the highly ordered $Ba(B'_{1/3}Nb_{2/3})O_3$ perovskites are quite alike with that of Ta-based counterparts.[11,15-20] Consequently, the highly ordered $Ba((Co, Zn, Mg)_{1/3}Nb_{2/3})O_3$ are taken as representative of $Ba(B'_{1/3}B''_{2/3})O_3$ perovskites to evaluate the ordered structure by TEM observation along various zone axes in the present work. The ordering feature and atomic configuration of each projection showed here are also applicable to Ta-based counterparts.

Experimental

$Ba((Co_{0.6-x/2}Zn_{0.4-x/2}Mg_x)_{1/3}Nb_{2/3})O_3$ (x = 0, 0.1, 0.2, 0.3) ceramics were prepared by a standard solid state reaction method from reagent-grade powders of $BaCO_3$ (99.93%), CoO (99.9%), ZnO (99.95%), MgO (99.9%) and Nb_2O_5 (99.99%). The weighed starting materials were mixed by ball milling with yttrium-stabilized zirconia media in ethanol for 24 h, and the mixtures were calcined at 1150 - 1200 °C in air for 3 h after drying. The calcined powders with 4 - 6 wt% polyvinyl alcohol (PVA) solution as binder were pressed into disks under a pressure of 98 MPa. The disks were sintered at 1475 - 1550 °C in air for 3 h to yield the dense ceramics. Then, the dense ceramics were annealed in air for 12 h at 1400 °C, 1450 °C and 1475°C, respectively. The samples after sintering and annealing were cooled at a rate of 2°C/min to 800°C, and then were cooled inside the furnace. Single phase with a hexagonal ($P\bar{3}m1$) symmetry is indexed for both the as-sintered and annealed samples after XRD step-scanning and Rietveld refinement.[9]

Samples with higher cation ordering degrees were chosen for TEM observation because of the accessibility to detect ordering. The structural feature and atomic configuration of an ordered area should be similar, unaffected by the compositions and treating conditions, since all of them share the same hexagonal symmetry. TEM samples were prepared by disaggregating the ceramics followed by grinding in an agate mortar. The powders were then suspended in acetone and dispersed onto a holey carbon 200 mesh TEM grid. TEM investigations were performed on 200 kV electron microscopy (Tecnai-F20, FEI Co., Hillsboro, Oregon).

Results and discussion

In order to gain a deep insight into the ordered structure of $Ba(B'_{1/3}B''_{2/3})O_3$ perovskites, TEM observation along a variety of important zone axes are necessary. A simple judgment of the feasibility of a zone axis is the SAED image should exhibit both the basic perovskite lattice and the superlattice. The superlattice is only observed along the variant, which is perpendicular to the beam direction for a given zone axis.[24]

The $<110>_c$ zone is the most informative and has been almost exclusively used to reveal the ordering characteristics and image the domain boundaries.[11,16-20] The following discussion on $<110>_c$ zone is based on the TEM images obtained in $Ba((Co_{0.5}Zn_{0.3}Mg_{0.2})_{1/3}Nb_{2/3})O_3$ sample after annealing at 1450°C. Fig. 1a shows SAED pattern along $<110>_c$ projection, the zone axis has been arbitrarily chosen as $[1\bar{1}0]_c$. For an given $[1\bar{1}0]_c$ zone axis, there are two sets of $<111>_c$

variants: $[111]_c$ and $[11\bar{1}]_c$ at the designated condition (marked by arrows).

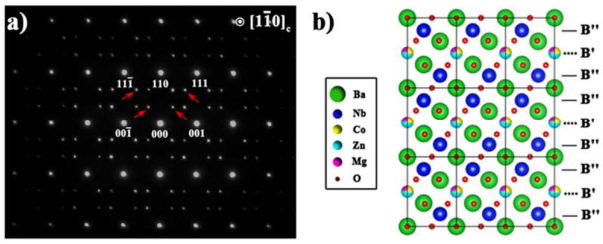

Fig. 1. a) SAED pattern viewed along $[1\bar{1}0]_c$ zone axis and b) schematic diagram of $<110>_c$ projection for ordered $Ba((Co, Zn, Mg)_{1/3}Nb_{2/3})O_3$ ceramics drawn with VENUS[25].

The priority of $[1\bar{1}0]_c$ zone axis to determine the ordered structure is for several reasons. Firstly, the occurrence of ±1/3{111}-type superlattice reflection directly reveals the 1:2 ordering, which happens along the $<111>_c$ direction. From this, a three-fold increase in the {111}-planer spacing of simple cubic unit cell occurs (0.71 nm = $3*d_{(111)c}$), which can be detected in high-resolution transmission electron microscopy (HRTEM) images. Secondly, along the $<110>_c$ projection, *B*-site cations do not overlap with other ions. The schematic diagram of $<110>_c$ projection for ordered $Ba((Co, Zn, Mg)_{1/3}Nb_{2/3})O_3$ ceramics is shown in Fig.1b. On this basis, deeper research by high-angle annular dark-field scanning transmission electron microscopy (HAADF STEM) can be operated, yielding both structural and chemical information at atomic resolution.[20-21,26] Finally and most importantly, it is quite convenient to detect the twin boundaries caused by orientational variants since two sets of $<111>_c$ variants exist for $<110>_c$ zone axis. [9,11]

Four types of twin boundaries with different orientations along $[1\bar{1}0]_c$ zone axis have been reported in our previous work.[9] Twin boundary with high energy is likely to form in ceramics with large domain size (> 200nm), leading to the deterioration of *Qf* values. Fig. 2 shows a type of twin boundary in the corresponding HRTEM image. The highly symmetrical twin boundary is conservative since cation disruption is quite small.[9] Ordered domain shows superperiod lattice with a periodicity of 0.71 nm. Each domain indicates one orientational variant (see the schematic SAED patterns in inset) and Fig. 1a is the final result after combination.[7,27-28] The upper-left area displays a periodicity of 0.41 nm, which is the lattice constant of fundamental cubic unit cell. Actually, area without superperiod is not always disordered. It has been proved as an ordered domain by a rotation of 90° around the $[001]_c$ axis by tilting experiments.[8] In consideration of the high ordering degree of samples in the present work[9,22], the upper-left area may also be an ordered domain, whose variant is not perpendicular to the beam direction of the given $[1\bar{1}0]_c$ zone axis.

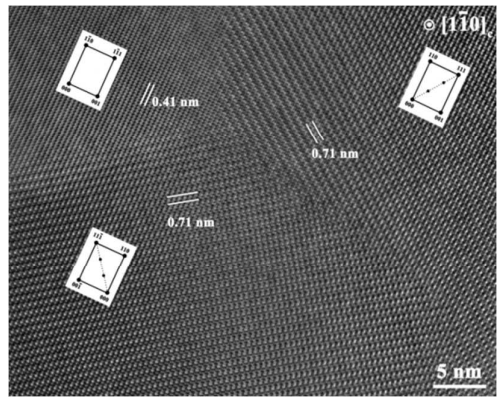

Fig. 2. HRTEM image viewed along $[1\bar{1}0]_c$ zone axis of $Ba((Co_{0.5}Zn_{0.3}Mg_{0.2})_{1/3}Nb_{2/3})O_3$ sample after annealing at 1450 °C.

It has been reported that twin boundaries separate the different orientational variants, while APBs separate the translational variants.[7-8,11] When viewed along $<110>_c$ zone axis, twin boundary is quite common, while APB is always combined with twin boundary,[17,27] which makes it much difficult to observe single APB. Thus another zone axis which can separate APB from twin boundary should be considered.

$<112>_c$ zone axis which also exhibits 1/3{111}-type superlattice reflections in its SAED image, has rarely been reported despite its feasibility for 1:2 ordering representation. TEM analysis along $<112>_c$ zone axis is carried out on the highly ordered as-sintered $Ba((Co_{0.5}Zn_{0.3}Mg_{0.2})_{1/3}Nb_{2/3})O_3$ sample. The SAED pattern viewed along $<112>_c$ direction is shown in Fig.3a, and zone axis is arbitrarily chosen as $[11\bar{2}]_c$. For each $<112>_c$ zone axis, there is only one set of $<111>_c$ variant, that means, visible domains are with the same orientation. In the corresponding HRTEM image in Fig. 3b, several ordered domains with superperiod of 0.71 nm, belong to the same $<111>_c$ variant. Meanwhile, domains close to the grain edge are easy to grow up as the elastic strains induced by the expansion of the superstructure release at the periphery.[7,29]

The enlarged lattice image of the marked area is shown in Fig. 3c. The fishbone like structure on the left side is approximately in agreement with the atomic configuration for ordered structure in Fig. 3d. The backbone is composed of *B′* columns, and the branches represent *B″* columns, columns with "…*B′*-*B″*- *B″*…" repetition come into being. Despite the nonexistence of the superperied lattice on the right side, it may also be an ordered domain, whose variant is not perpendicular to the given zone axis. The interface between them is an orientation domain boundary, and tilting experiment is required to determine the orientation rotation.

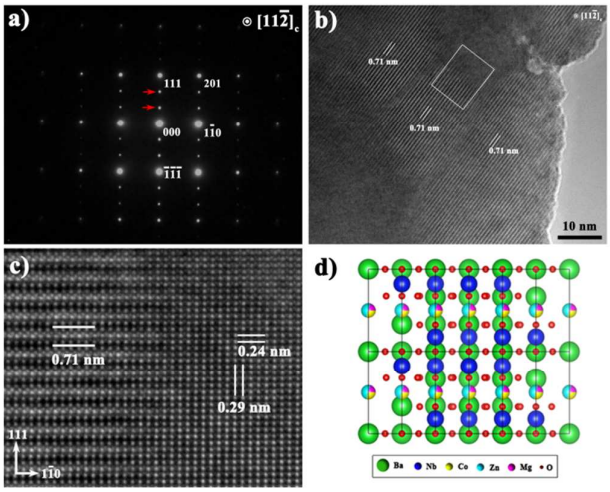

Fig. 3. TEM images of the as-sintered $Ba((Co_{0.5}Zn_{0.3}Mg_{0.2})_{1/3}Nb_{2/3})O_3$ sample: a) SAED pattern and b) HRTEM image viewed along $[11\bar{2}]_c$ zone axis; c) Higher amplification lattice image of the marked area. d) Schematic diagram of $<112>_c$ projection for ordered $Ba((Co, Zn, Mg)_{1/3}Nb_{2/3})O_3$ ceramics drawn with VENUS[25].

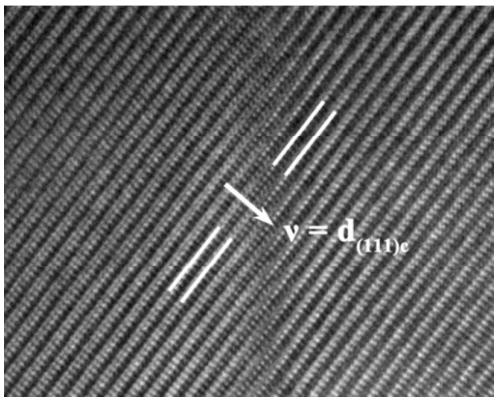

Fig. 4. HRTEM image showing anti-phase relationship along $[11\bar{2}]_c$ zone axis.

When viewed along $<112>_c$ zone axis, there is only one set of $<111>_c$ variant, twin boundaries will not intersperse with APBs because of the invisibility. As a result, single APBs, which form between regions nuclear on the same set of $\{111\}_c$ planes but out of phase, are quite convenient to be observed. Fig. 4 gives the HRTEM image showing anti-phase relationship along zone axis $[11\bar{2}]_c$. A dislocation with a distance of a third of 0.71 nm appears at the boundary, the displacement vector is $\nu = d_{(111)c}$.

The 1:2 ordering is directly revealed by the appearance of ±1/3{111}-type superlattice spots in $<110>_c$ and $<112>_c$ zone axis. However, $<111>_c$ zone axis which exhibits ±1/3{112}-type superlattice reflections, has also been used to evaluate the 1:2 ordered structure occasionally.[8,19,30] The feasibility of the indirect method is urgently to be proved. Meanwhile, it is noteworthy that the projection is parallel to the ordering direction, the corresponding HRTEM image is worth investigating since it should contain rich structural information different from others.

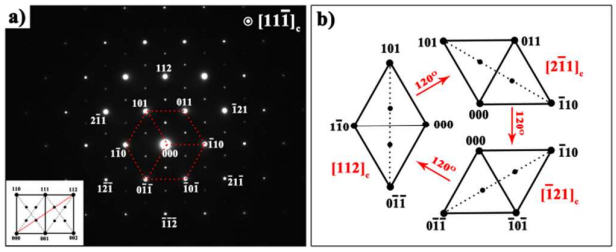

Fig. 5. SAED pattern viewed along $[11\bar{1}]_c$ zone axis and b) schematic diagram of the relationship between $<112>_c$ orientations around $[11\bar{1}]_c$ axis.

To detect the ordering characteristics along $<111>_c$ zone axis, $Ba((Co_{0.45}Zn_{0.25}Mg_{0.3})_{1/3}Nb_{2/3})O_3$ sample after annealing at 1400 °C was arbitrarily chosen. SAED pattern viewed along zone axis $[11\bar{1}]_c$ is shown in Fig. 5a, the superlattice spots lies along $<112>_c$ direction. Inset shows the SAED sketch map of $<110>_c$ zone, from which $\pm1/3\{112\}_c$ superlattice spots can be derived and they come from the same set of one $<111>_c$ variant. (marked by the red dotted line) Therefore, $\pm1/3\{112\}_c$ superlattice spots can also be treated as a signature to detect *B*-site ordering. There are 4 equivalent $<111>_c$ directions and 12 equivalent $<112>_c$ directions for the cubic perovskite cell. One given $[111]_c$ zone axis corresponds to three equivalent ordered $<112>_c$ directions. When the zone axis is arbitrarily chosen as

$[11\bar{1}]_c$, these are $[112]_c$, $[\bar{1}21]_c$ and $[2\bar{1}1]_c$. The relationship between these $<112>_c$ directions is shown in Fig. 5b, displaying a rotation of 120° around the $[11\bar{1}]_c$ axis.

Fig. 6a shows the HRTEM image of $Ba((Co_{0.45}Zn_{0.25}Mg_{0.3})_{1/3}Nb_{2/3})O_3$ sample after annealing at 1400 °C viewed along $[11\bar{1}]_c$ zone axis. The high magnification images of the labeled areas are shown in Fig. 6b and 6c. Area I displays a superlattice with a modulation of 0.50 nm, which is about the triple of the {112}-planer spacing of simple cubic unit cell (0.50 nm ~ $3*d_{(112)c}$). In the ordered area along the given $[11\bar{1}]_c$ zone axis, three ordered $<112>_c$ directions co-exists with each other. In order to interpret the component-related image contrast, simulated HRTEM image is performed along $<111>_c$ zone axis by using Java Electron Microscopy Software (JEMS).[31] (see Fig. 6d) There is an excellent match between the simulated HRTEM image with the experimental data. Meanwhile, the schematic diagram showing the atomic configuration of ordered structure is shown in Fig. 6e. Atomic positions of *B*-site cations are overlap with these of Ba columns, which exhibits a highest Z (56) value. By comparing the *B*-site atomic positions with HRTEM image, the brighter spots have the correct configuration and positions to represent *B′* columns (Co, Zn and Mg) and the less bright spots correspond to *B″* columns (Nb). The contrast does not match with Z-contrast image, whose intensity is proportional to Z^2.[32] Actually, HRTEM image shows many different forms depending on the crystal thickness and microscope focus.[33-34] From the above, the 1:2 ordered structure can be confirmed, columns giving "…*B′*-*B″*- *B″*…" sequence is detected along the three $<112>_c$ directions (marked by red rectangles in Fig. 6b). The brighter *B′* columns connected by red dotted lines form an outside hexagon, inside which a smaller hexagon connecting the less bright *B″* columns with yellow dotted lines exists. Thus the 1:2 ordered structure with hexagonal symmetry is confirmed clearly.

Area Π shows basic cubic lattice along the given $[11\bar{1}]$ zone axis. With the absent of contrast, Fig. 6c exhibits lattice with a modulation of 0.28 nm, which is the {110}-planer spacing of simple cubic unit cell. The simulated HRTEM of disordered structure is shown in Fig. 6f, coinciding with the experimental data. Nevertheless, as discussed in the preceding section, area Π may also be an ordered domain. The orientation rotation between Area I and Area Π is supposed to be either 90° or 180°, which can be further determined by tilting experiment.

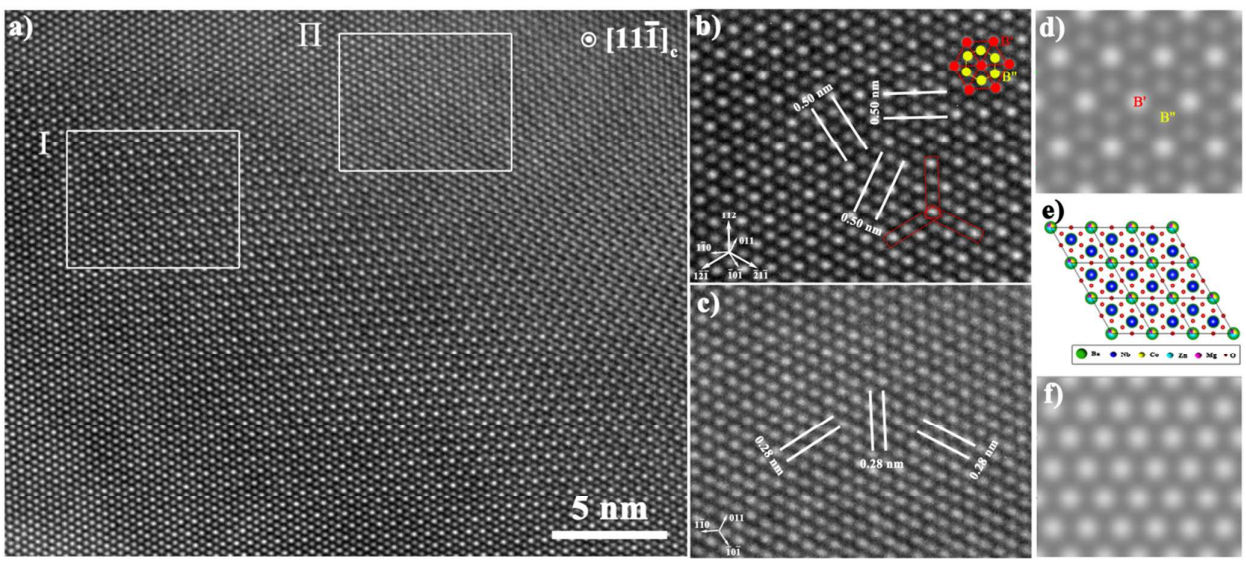

Fig. 6. a) The corresponding HRTEM image viewed along $[11\bar{1}]_c$ zone axis and higher amplification lattice image of the labeled areas: b) area I; c) area Π. Simulated HRTEM image for d) 1:2 ordered and f) disordered $Ba(B'_{1/3}B''_{2/3})O_3$ perovskites with defocus d = 110 nm and thickness t = 4.3 nm along $<111>_c$ zone axis. e) Schematic diagram of $<111>_c$ projection for ordered $Ba((Co, Zn, Mg)_{1/3}Nb_{2/3})O_3$ ceramics drawn with VENUS[25].

Journal Name

ARTICLE

When ordering happens, the c-axis of the ordered hexagonal structure lies arbitrary along one of the four equivalent $<111>_c$ directions, which are with the same probability. From the above discussion, for each zone axis, there is a certain proportion of ordered area invisible in the corresponding HRTEM image. For a completely ordered sample, the theoretical proportion of the invisible ordered area is 1/2 ($<110>_c$), 3/4 ($<111>_c$) and 3/4 ($<112>_c$) respectively.

Conclusions

TEM observations along several zone axes could be used to evaluate the 1:2 ordered structure in $Ba(B'_{1/3}B''_{2/3})O_3$ perovskites, and each zone axis has its own advantage and special ordering feature. For zone axis $<110>_c$ and $<112>_c$, the 1:2 ordered structure is directly determined by the occurrence of 1/3{111}-type superlattice reflections in their corresponding SAED images. The most informative $<110>_c$ zone gives two sets of $<111>_c$ ordering variants, showing a twin relationship between domains. While there is only one set of $<111>_c$ variant along the $<112>_c$ projection, it is quite convenient to detect the anti-phase relationship between domains. The 1/3{112}-type superlattice reflections observed along $<111>_c$ zone axis, can also be treated as an ordering signature. As the projection is parallel to the ordering direction, the corresponding HRTEM image clearly shows the 1:2 ordered structure with hexagonal symmetry. Since ordering lies along one of the four equivalent <111> directions of the parent cubic cell, ordered domains whose variants are not perpendicular to the given zone axis are invisible in the corresponding HRTEM images. For a completely ordered sample, the theoretical proportion of ordered area invisible for each zone axis is 1/2 ($<110>_c$), 3/4 ($<111>_c$) and 3/4 ($<112>_c$), respectively.

Acknowledgements

The present work was supported by National Natural Science Foundation of China under grant number 11274270 and Chinese National Basic Research Program under grant number 2015CB654601. The authors would like to acknowledge Dr. Juan Juan Xing and Dr. Dong Li Hu at School of Materials Science and Engineering, Shanghai University, Dr. Fa Qiang Zhang at Shanghai Institute of Ceramics, Chinese Academy of Sciences, for their valuable advices on TEM analysis.

Notes and references

1. T. A. Vanderah, "Talking Ceramics," *Science* 2002, **298**, 1182-1184.

2. I. M. Reaney, D. Iddles, "Microwave Dielectric Ceramics for Resonators and Filters in Mobile Phone Networks," *J. Am. Ceram. Soc.,* 2006, **89**, 2063-2072.

3. S. Kawashima, M. Nishida, I. Ueda, H. Ouchi, "$Ba(Zn_{1/3}Ta_{2/3})O_3$ Ceramics with Low Dielectric Loss at Microwave Frequencies," *J. Am. Ceram. Soc.,* 1983, **66**, 421-423.

4. P. K. Davies, H. Wu, A.Y. Borisevich, I. E. Molodetsky, L. Farber, "Crystal Chemistry of Complex Perovskites: New Cation-Ordered Dielectric Oxides," *Annu. Rev. Mater. Res.* 2008, **38**, 369-401.

5. F. Galasso, L. Katz, R. Ward, "Substitution in the Octahedrally Coordinated Cation Positions in Compounds of the Perovskite Type," *J. Am. Chem. Soc.* 1959, **81**, 820-823.

6. M. W. Lufaso, "Crystal Structure, Modeling, and Dielectric Property Relationships of 2:1 Ordered $Ba_3MM'_2O_9$ (M = Mg, Ni, Zn; M' = Nb, Ta) Perovskites," *Chem. Mater.*, 2004, **16**, 2148-2156.

7. I. M. Reaney, I. Qazi, W. E. Lee, "Order-disorder Behavior in $Ba(Zn_{1/3}Ta_{2/3})O_3$" *J. Appl. Phys.,* 2000, **88**, 6708-6714.

8. C. H. Lei, G. Vantendeloo, S. Amelinckx, "The Microstructure of Ordered $Ba(Mg_{1/3}Ta_{2/3})O_3$," *Philos. Mag. A*, 2002, **82**, 349-367.

9. P. P. Ma, L. Yi, X. Q. Liu, L. Li, X. M. Chen, "Effects of Post-densification Annealing upon Microstructures and Microwave Dielectric Characteristics in $Ba((Co_{0.6-x/2}Zn_{0.4-x/2}Mg_x)_{1/3}Nb_{2/3})O_3$ Ceramics," *J. Am. Ceram. Soc.,* 2013, **96**, 3417-3424.

10. G. V. Tendeloo, S. Amelinckx, "Group-theoretical Considerations Concerning Domain Formation in Ordered Alloys," *Acta Cryst. A*, 1974, **30**, 431-440.

11. P. K. Davies, J. Z. Tong, "Effect of Ordering-Induced Domain Boundaries on Low-Loss $Ba(Zn_{1/3}Ta_{2/3})O_3$-$BaZrO_3$ Perovskite Microwave Dielectrics," *J. Am. Ceram. Soc.,* 1997, **80**, 1727-1740.

12. E. Schlömann, "Dielectric Losses in Ionic Crystals with Disordered Charge Distributions," *Phys. Rev.*, 1964, **135**[2] A413-419.

13. H. Tamura, "Microwave Dielectric Losses Caused by Lattice Defects," *J. Eur. Ceram. Soc.,* 2006, **26**, 1775-1780.

14. H. Tamura, T. Konoike, Y. Sakabe and K. Wakino, "Improved High-*Q* Dielectric Resonator with Complex Perovskite Structure," *J. Am. Ceram. Soc.*, 1984, **67**, C59-61.

15. C. T. Lee, Y. C. Lin, C. Y. Huang, C. Y. Su and C. L. Hu, "Cation Ordering and Dielectric Characteristics in Barium Zinc Niobate," *J. Am. Ceram. Soc.*, 2007, **90**, 483-489.

16. M. S. Fu, X. Q. Liu, X. M. Chen and Y. W. Zeng, "Effects of Mg-Substitution on Microstructures and Microwave Dielectric Properties of $Ba(Zn_{1/3}Nb_{2/3})O_3$ Perovskite Ceramics," *J. Am. Ceram. Soc.,* 2010, **93**, 787-795.

17. C. F. Lin, H. H. Lu, T. I. Chang, J. L. Huang, "Influence of Superlattice and Antiphase Domain Boundaries on Dielectric Loss in $Ba[Mg_{1/3}(Nb_{x/4}Ta_{(4-x)/4})_{2/3}]O_3$ Ceramics," *Appl. Phys. Lett.,* 2005, **87**, 102905-1-3.

18. H. J. Youn, K. Y. Kim and H. Kim, "Microstructural Characteristics of $Ba(Mg_{1/3}Ta_{2/3})O_3$ Ceramics and Its Related Microwave Dielectric Properties," *Jpn. J. Appl. Phys.*, 1996, **35**, 3947-3953.

19. J. Sun, S. J. Liu, N. Newman and D. J. Smith, "Atomic Resolution Transmission Electron Microscopy of the Microstructure of Ordered $Ba(Cd_{1/3}Ta_{2/3})O_3$ Perovskite Ceramics," *J. Am. Ceram. Soc.,* 2006, **89**, 1047-1052.

20. F. Azough, R. Freer, D. Iddles, T. Shimada and B. Schaffer, "The Effect of Cation Ordering and Domain Boundaries on Low Loss $Ba(B^{I}_{1/3}B^{II}_{2/3})O_3$ Perovskite Dielectrics Revealed by High-angle Annular Dark-field Scanning Transmission Electron Microscopy (HAADF STEM),"*J. Eur. Ceram. Soc.,* 2014, **34**, 2285-2297.

21. Y. Yan, S. J. Pennycook, Z. Xu and D. Viehland, "Determination of the Ordered Structures of $Pb(Mg_{1/3}Nb_{2/3})O_3$ and $Ba(Mg_{1/3}Nb_{2/3})O_3$ by Atomic-resolution Z-contrast Imaging," *Appl. Phys. Lett.,* 1998, **72**, 3145-3147.

22. P. P. Ma, L. Yi, X. Q. Liu, L. Li and X. M. Chen, "Effects of Mg-Substitution on Order/disorder Transition, Microstructure and Microwave Dielectric Characteristics of $Ba((Co_{0.6}Zn_{0.4})_{1/3}Nb_{2/3})O_3$ Complex Perovskite Ceramics," *J. Am. Ceram. Soc.,* 2013, **96**, 1795-1800.

23. R. D. Shannon, ''Revised Effective Ionic Radii and Systematic Studies of Interatomic Distances in Halides and Chalcogenides,'' *Acta Crystal., Sect. A: Cryst. Phys. Diffr., Theor. Gen. Crystallogr.*, 1976, **A32**, 751-767.

24 J. Sun, S. J. Liu, N. Newman and D. J. Smith, "Ordered Domains and Boundary Structure in $Ba(Cd_{1/3}Ta_{2/3})O_3$ Perovskite Dielectrics," *Appl. Phys. Lett.,* 2004, **84**, 3918-3920.

25. F. Izumi and R. A. Dilanian, "Recent Research Development in Physics," vol. 3, Part Π, Transworld Research Network, Trivandrum, ISBN 81-7895-046-4, 2002, pp. 699 - 726.

26. S. J. Pennycook and P. D. Nellist, Z-contrast Scanning Transmission Electron Microscopy, in: D. G. Rickerby, U. Valdré, and G. Valdré (Eds.), Impact of Electron and Scanning Probe Microscopy on Materials Research., Kluwer Academic Publishers, Dordrecht, 1999, pp. 161-207.

27. C. F. Lin, H. H. Lu, T. I. Chang and J. L. Huang, "Effect of Ordered Structure and Domain Boundary on Low-loss $Ba[Mg_{1/3}(Nb_{x/4}Ta_{(4-x)/4})_{2/3}]O_3$ Microwave Dielectric Ceramics," *J. Mater. Res.,* 2006, **21**, 2564-2571.

28. Y. W. Kim, J. H. Park and J. G. Park, "Local Cationic Ordering Behavior in $Ba(Mg_{1/3}Nb_{2/3})O_3$ Ceramics," *J. Eur. Ceram. Soc.*, 2004, **24**, 1775-1779.

29. H. Wu and P. K. Davies, "Influence of Non-Stoichiometry On the Structure and Properties of $Ba(Zn_{1/3}Nb_{2/3})O_3$ Microwave Dielectrics: II. Compositional Variation in Pure BZN," *J. Am. Ceram. Soc.*, 2006, **89**, 2250-2263.

30. D. J. Barber, K. M. Moulding, J. I. Zhou and M. Q. Li, "Structural Order in $Ba(Zn_{1/3}Ta_{2/3})O_3$, $Ba(Zn_{1/3}Nb_{2/3})O_3$ and $Ba(Mg_{1/3}Ta_{2/3})O_3$ Microwave Dielectric Ceramics," *J. Mater. Sci.*, 1997, **32**, 1531-1544.

31. P. Stadelmann, JEMS: Java Electron Microscopy Software. Available from: http://cime.epfl.ch 2007.

32. S. J. Pennycook, Structure Determination through Z-contrast Microscopy, in: P.W. Hawkes (Ed.), Advances in Imaging and Electron Physics, Microscopy, Spectroscopy, Holography and Crystallography with Electrons, vol. 123, Elsevier Academic Press Inc., San Diego, 2002, pp. 173-206.

33. S. J. Pennycook, "Z-Contrast Transmission Electron Microscopy: Direct Atomic Imaging of Materials," *Annu. Rev. Maler. Sci.*, 1992, **22**, 171-195.

34. M. O. Beeck, D. V. Dyck, "Direct Structure Reconstruction in HRTEM," Ultramicroscopy, 1996, **64**, 153-165.

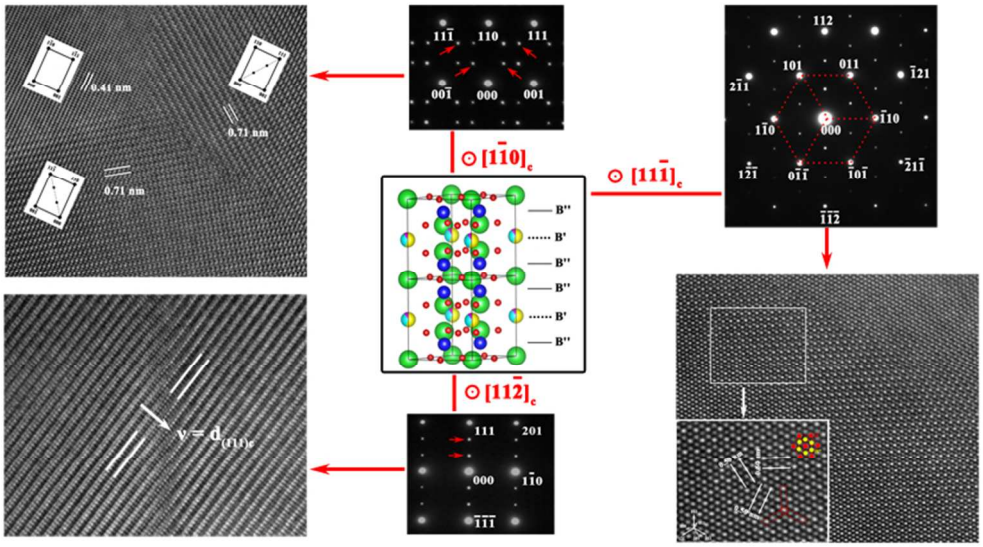

71x39mm (300 x 300 DPI)